Atmospheric circulation changes and neoglacial conditions in the Southern Hemisphere mid-latitudes: insights from PMIP2 simulations at 6 kyr

Maisa Rojas · Patricio I. Moreno

Abstract Glacial geologic studies in the Southern Hemisphere (SH) mid-latitudes (40–54°S) indicate renewed glacial activity in southern South America (Patagonia) and New Zealand's (NZ) South Island starting at ∼7 kyr, the so-called neoglaciation. Available data indicate that neoglacial advances in these regions occurred during a rising trend in atmospheric CO_2 and CH_4 concentrations, lower-than-present but increasing summer insolation and seasonality contrasts. In this paper we examine the climatological context in which neoglaciations occurred through analysis of the complete Paleoclimate Modelling Inter-comparison Project (PMIP2) database of simulations at 6 kyr for the SH. We observe that the amplitude of the annual insolation cycle in the SH did not change significantly at 6 kyr compared to the pre-industrial values, the largest difference occurring in autumn (MAM, negative anomalies) and spring (SON, positive anomalies). The simulated changes in temperatures over the SH respond to the insolation changes, with a 1–2 month delay over the oceans. This results in a reduced amplitude of the annual cycle of temperature and precipitation over most continental regions, except over Patagonia and NZ, that show a slight increase. In contrast, large-scale circulation features, such as the low and upper level winds and the subtropical anticyclones show an amplified annual cycle, as a direct response to the increased/decreased insolation during the transitional seasons SON/MAM. In the annual mean, there is a small but consistent equatorward shift of the latitude of maximum wind speed of 1–3° over the entire SH, which results in a small increase of wind speed over the South Pacific and Atlantic Oceans north of ∼50°S and a widespread decline south of 50°S. PMIP2 simulations for 6 kyr, indicate that in the annual mean, the SH mid-latitudes were colder, wetter and with stronger winds north of about 50°S. These conditions are consistent with the observed neoglacial advances in the region, as well as with terrestrial paleoclimate records from Patagonia that indicate cooling and a multi-millennial rising trend in Southern Westerly Wind intensity starting at ∼7.8 kyr.

1 Introduction

Glacial geologic studies in the southern mid-latitudes (40–54°S) indicate renewed glacial activity in southern South America (western Patagonia) and New Zealand's (NZ) South Island during the most recent half of the Holocene epoch, the so-called neoglaciation (e.g. Porter 2000). These data indicate that neoglacial advances started at 7–6 kyr in Patagonia and probably slightly earlier in NZ (e.g. Schaefer et al. 2009), featured multiple advances at sub-millennial timescales, and culminated with advance of alpine glaciers in both regions at a similar time as the European Little Ice Age. Neoglaciation occurred during a rising trend in atmospheric CO_2 and CH_4 concentrations, lower-than-present but increasing summer insolation and seasonality contrasts; at times when sea level and coastline configurations were approaching modern-day condition at a global

M. Rojas (✉)
Department of Geophysics, University of Chile,
Blanco Encalada 2002, Santiago, Chile
e-mail: maisa@dgf.uchile.cl

P. I. Moreno
Department of Ecology, University of Chile,
Las Palmeras, Santiago, Chile

scale. Available paleoclimate data from the Southern Hemisphere (SH) mid-latitudes indicate that neoglaciation activity is immersed in a multi-millennial trend toward increasing precipitation and surface wind speeds (Gilli et al. 2005; Moreno 2004; Shulmeister et al. 2004) starting at ∼7.8 kyr and lower-than-present sea surface temperatures (Lamy et al. 2001). These conditions contrast with the preceding early Holocene (11.5–8 kyr) minimum in precipitation of westerly origin (Abarzua et al. 2004; Massaferro and Brooks 2002; Moreno 2004), and maxima in temperature and fire activity in Patagonia (Whitlock et al. 2007). The contrasting behaviour of glaciers in the Southern and Northern Hemisphere during neoglaciations, recently discussed by Schaefer et al. (2009), suggests that regional controls such as atmospheric circulation changes could be a key factor modulating hemispheric-scale glacial behaviour during the Holocene. For example, Fitzharris et al. (2007) found distinct synoptic-scale as well as hemispheric scale conditions (large-scale SH modes of variability such as the Southern Annular Mode and the Interdecadal Pacific Oscillation) associated with advance and retreat phases of glaciers in the Southern Alps during the twentieth century, that are also broadly coherent with changes in Southern Patagonian glaciers.

The majority of climate modelling studies during the Holocene, however, have aimed at understanding the steady state climate conditions at 6 kyr, in particular the effects of changes in the annual insolation cycle on the monsoonal systems of the world (e.g. Kutzbach and Liu 1997; Liu et al. 2004). The results of these simulations compare well with low-latitude paleoclimate data and provide insights into the circulation basis underlying paleoclimate change. One important finding of those modelling studies is that enhanced insolation seasonality, resulting from an orbitally shifted timing of insolation minima and maxima during the annual cycle, increased the land/ocean temperature contrasts and consequently enhanced monsoonal circulation (Wohlfahrt et al. 2004; Kutzbach and Liu 1997). According to Braconnot et al. (2007a) the changes in the climate triggered by insolation forcing at 6 kyr were more attenuated in the SH.

A notable exception to the mid-Holocene Monsoonal focus is a study by Wagner et al. (2007), who carried out a transient simulation with a coupled atmosphere–ocean model for the interval between 7.4–4.5 kyr and focused their analysis on the extra-Andean sector of southeastern Patagonia (52°S, 70°W). The aim of their analysis was to investigate the linkage between large-scale circulation and precipitation in that region. Their simulations indicate stronger SH westerly winds during austral summer and weaker winds during austral winter, and conclude that the local circulation/precipitation relationship found in their simulation was inconsistent with the lower lake levels

interpreted from sedimentary data retrieved from lake Potrok Aike (52°S, 70°W, Wagner et al. 2007). In this study we examine the response of the SH climate to the insolation regime at 6 kyr, and its relationship with neoglacial activity in the southern mid-latitudes. For that purpose we present a series of paleoclimate simulations performed in the context of the Paleoclimate Modeling Intercomparison Project 2 (PMIP2).

2 Models and experiments

We analysed the complete PMIP2 database of 6 kyr simulations (13 coupled Ocean–Atmosphere models, AO-GCMs), which were run using pre-industrial (PI, hereafter) greenhouse gas concentrations, present day sea-ice distribution, sea surface level, topography and vegetation. There are two differences in radiative forcing of these simulations relative to PI. First the changes in seasonal insolation, calculated from the orbital configuration at 6 kyr. Secondly, methane values are set to 650 ppb, instead of 760 ppb used in the control simulations. The rest of the Greenhouse Gases (GHG, CO_2, NO_2, CFC, O_3) held at the same value as in the PI simulations. Note that this choice of GHG concentrations for 6 kyr are not exact, especially in terms of CO_2, which should be slightly lower (269 ppb, Monnin et al. 2004). All models are fully coupled and include at least the following components: atmosphere, ocean, land surface, and sea-ice. Table 1 lists general characteristics of the atmospheric and oceanic components of these models. We analysed the control simulations (PI) and the climate simulations centred at 6 kyr. Both simulations were run for long enough to allow the atmosphere and oceans to adapt to the specified boundary conditions until they reached a quasi-equilibrium state devoid of trends. More information on the setup of these experiments and validation can be found on the PMIP2 webpage (http://pmip2.lsce.ipsl.fr/) and in Braconnot et al. (2007a).

The analyses carried out and presented in this paper were done for the ensemble mean monthly mean data. To get the ensemble mean, we first re-gridded all the fields to a common 1 × 1 degree grid, and then took the average. To assert the significance of some of the evaluated changes, we performed significance tests (student t) on the 6 kyr-PI differences between the means. Another way to asses significance was done by the means of boxplots, that indicate the model spread about the median (Figs. 9, 11).

We focus our analysis on two mountain regions in the SH mid-latitudes (40–54°S): the Southern Andes in southern South America (Patagonia hereafter) and the Southern Alps of New Zealand (NZ hereafter). Both are topographically complex and longitudinally narrow regions represented as wider and lower by the resolution coarseness

Table 1 PMIP2 coupled ocean–atmosphere models employed in this analysis

Model name	Atmosphere res lon × lat	Vertical levels	Ocean lon × lat	Vertical levels
CCSM3.0 ver beta14	1.4 × 1.4	26	∼1 × 1	40
MIROC3.2	2.8 × 2.8	20	1.4 × 1.4	43
MRI-CGCM2.3.4fa	2.8 × 2.8	30	2.5 × 2.0 (0.5 tropics)	31
MRI-CGCM2.3.4nfa	2.8 × 2.8	30	2.5 × 2.0 (0.5 tropics)	31
FGOALS-1.0g	2.8 × 2.8	26	1 × 1	31
ECHAM5-MPIOM1	3.75 × 2.5	20	1.0 × 1.0	41
ECHAM5e-MPIOM127-LPJ	3.75 × 2.5	19	1.5 × 1.5	40
IPSL-CM4	3.75 × 2.5	19	2.4 × 2.4 $\cos\phi$	31
UBRIS-HadCM3M2	3.75 × 2.5	19	1.25 × 1.25	19
GISSmodelE	5 × 4	20	5 × 4	31
CSIRO-Mk3Lv1.0	5.625 × ∼3.18	18	2.8125 × ∼1.59	21
CSIRO-Mk3Lv1.1	5.625 × ∼3.18	18	2.8125 × ∼1.59	21
FOAM	7.5 × 4.5	18	2.8125 × 1.4	24

of regular AO-GCMs (see Table 1). For several quantities we will present area-averaged quantities employing the boundaries of these two regions, but considering only the area above 500 m of the individual model topographies.

2.1 Orbital forcing

Differences in orbital parameters during the Holocene produced changes in the seasonal cycle of solar radiation. Figure 1 shows the monthly mean insolation anomalies (6 kyr-PI) as a function of latitude, along with the averaged insolation curves over the SH (20–70°S) for the same time-slice. Higher-than-present obliquity at 6 kyr led to an increase in insolation at high latitudes (>60°) in both hemispheres; this factor, coupled with a late-August perihelion, led to peak positive anomalies in insolation between August–September in the SH and June–July in the Northern Hemisphere (NH) (see figure 2 of Braconnot et al. 2007a for the NH). Strong negative insolation anomalies developed during January–February throughout the entire SH, whilst relatively weak anomalies developed in the NH between September and May. These changes reduced the insolation seasonality in the SH while enhancing it in the NH (Braconnot et al. 2007a). The southern mid-latitudes in particular (30–50°S), exhibit negative insolation anomalies from November through March, and positive anomalies from June to October. The positive anomalies increase poleward and reach the largest values between mid-August to mid-October in areas south of 70°S (Fig. 1a). An additional effect of the orbital change at 6 kyr is a change in the length of the seasons. However, in the PMIP2 experimental setup protocol it was decided to keep the definition of seasons with the same calendar as the control simulation. This leads to an overestimation of the insolation differences between 6 kyr and PI of ∼15 W/m^2

during autumn in the SH (and an underestimation in the NH for the same period, Joussaume and Bracconnot 1997).

3 Results

We calculated the ensemble mean of all 13 simulations and assessed the changes in temperature, sea level pressure, circulation, and precipitation for all seasons relative to the PI simulations. In the following section we describe the results of these simulations at hemispheric scale, and then focus on southern South America (Patagonia) and New Zealand (NZ) to evaluate the impact of the 6 kyr boundary conditions on the climate of these regions, considering the presence of ice fields in the critical region of the Southern Westerly Winds, and reports of neoglacial activity. For an evaluation of the control simulations refer to Braconnot et al. (2007a) and Rojas et al. (2009).

3.1 Temperature

Figure 2 shows the seasonal and annual mean surface temperature differences (6 kyr-PI) in the SH. The results indicate at 6 kyr colder conditions over the continents during austral Summer (DJF) and Autumn (MAM), compared to PI. During austral Winter (JJA) the central part of the continents are warmer than present while their southern tips exhibit negative anomalies. Compared to the corresponding PI season, during Spring (SON), all continental regions, including Antarctica, show strong positive temperature anomalies (between 1 and 2°), and the same applies to most of the ocean surface (up to 0.5°). The air temperatures over the oceans show predominantly colder conditions during MAM, except for a widespread warm anomaly in the Southern Ocean >50°S particularly evident

Fig. 1 Insolation: **a** 6 kyr-PI, **b** Southern Hemisphere (30–60°S) average PI and 6 kyr insolation
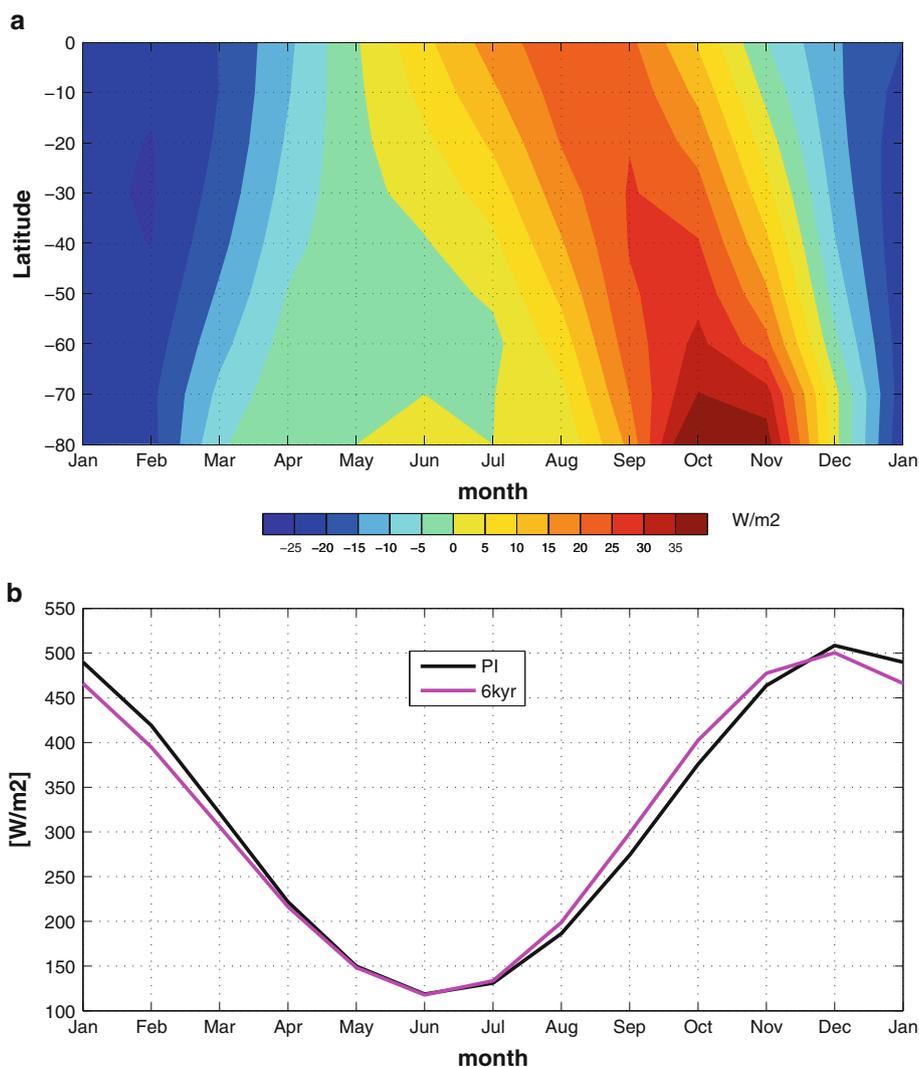
in the Weddell Sea. This positive anomaly expands northward during JJA, becomes extensive throughout the SH during SON, and starts to vanish southward during DJF. When averaged over the course of the year, the results point to predominantly colder oceans and continents north of 45–50°S, depending on the ocean basin, and predominantly warmer conditions toward the south compared to PI. Our regions of interest, Patagonia and NZ, were colder in the annual mean. In summary, we see fairly longitudinally homogeneous changes over the SH between 0 and 50°S. The continents were colder than PI, between Dec–May, and warmer than PI between Jul–Nov, note that the period when the continents were colder (Dec–May) roughly coincides with the ablation season in NZ and Patagonia.

Sea surface temperature (SST, not shown) changes resemble the surface air temperatures. SSTs were warmer during DJF and SON at 6 kyr, and colder during the remainder of the year. In the annual mean the Southern

Oceans north of ∼60°S were colder, and warmer south of that compared to PI.

3.2 Sea level pressure

Figure 3 shows the ensemble mean seasonal mean sea level pressure (SLP) for both 6 kyr and PI simulations (contours) and their respective seasonal differences (colour shading) in the SH. The models reproduce the permanent anticyclones on the eastern margin of the three ocean basins in the SH and over eastern Antarctica. The SLP difference (6 kyr-PI) fields are smallest during DJF, and give way to a widespread negative anomaly between 40–55°S and a positive anomaly south of this region during MAM. The latter differences expand over the entire Pacific Ocean during JJA while negative differences develop over central Africa and the Indian Ocean sector south of it. Higher SLP at 6 kyr, compared to PI, persists in the central Pacific

Fig. 2 Model mean surface temperature differences, 6 kyr-PI: **a** DJF, **b** MAM, **c** JJA, **d** SON, **e** Annual mean
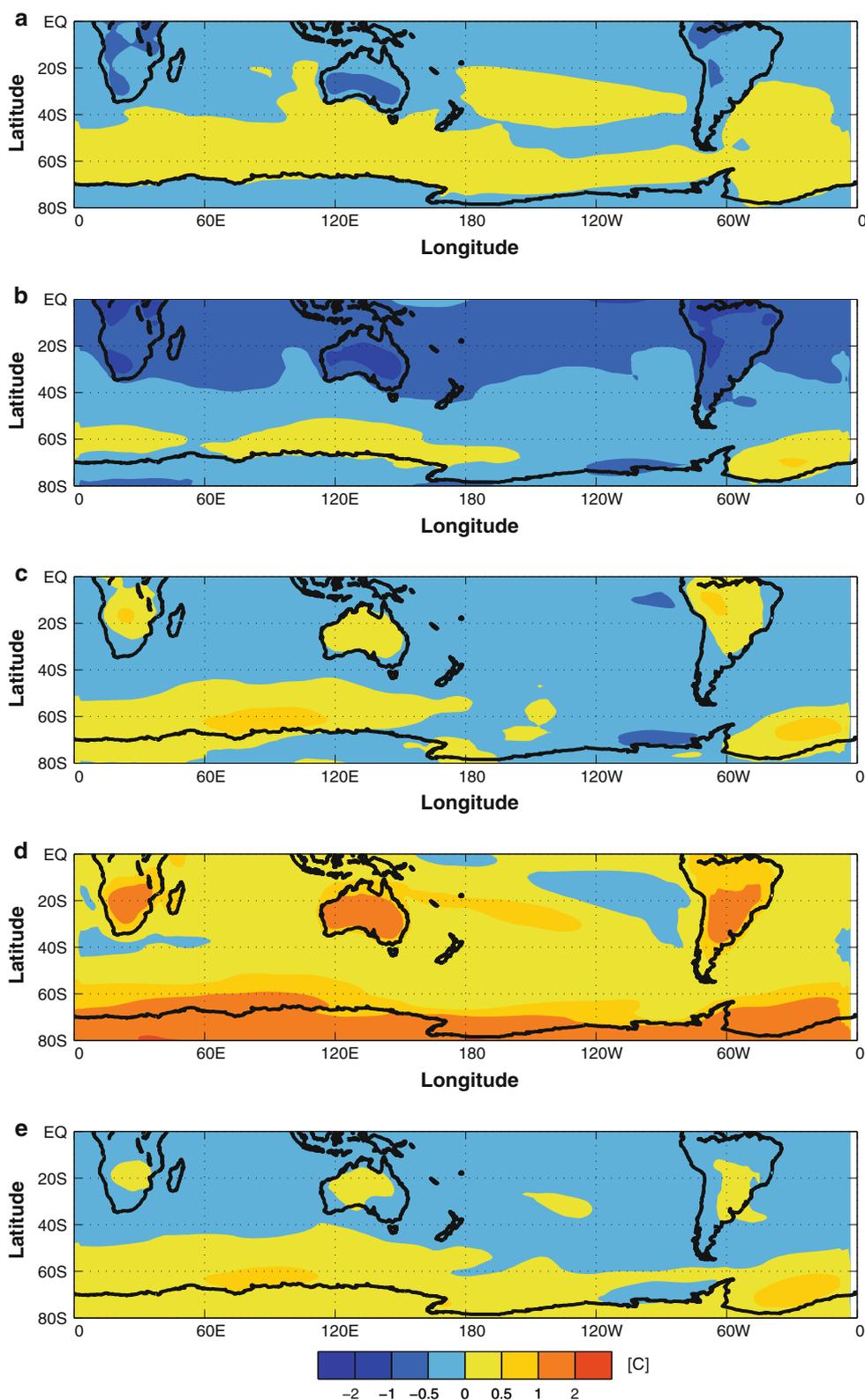
Ocean north of 45°S and the Southern Ocean sector south of Australia (40–60°S) during SON, the African anomaly also persists and expands eastward, and lower than PI SLP develop over eastern Antarctica, the Pacific sector of the Southern Ocean, most of Australia and central South America.
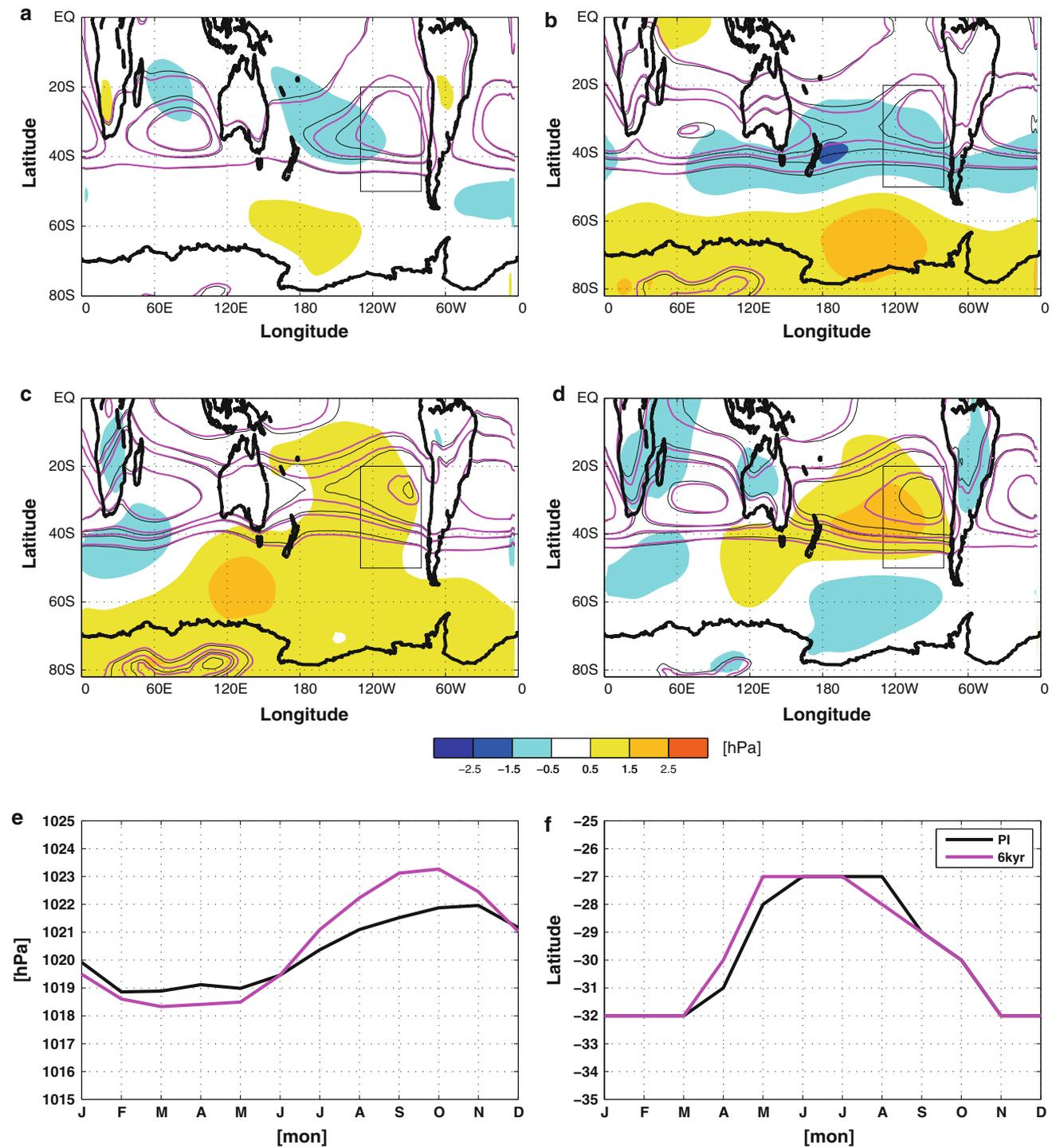
Fig. 3 Model mean sea level pressure changes: 6 kyr-PI, **a** DJF, **b** MAM, **c** JJA, **d** SON. Annual cycle of: **e** maximum SLP over the region of the Pacific anticyclone (*box* in parts a–d), **f** latitude of maximum SLP

The above described SLP anomalies over the South Pacific lead to a lower SLP gradient in the 6 kyr simulations compared to PI in this region during MAM (Fig. 3), whereas the SLP anomaly in SON produces an increased SLP gradient. These changes in the SLP gradients will, in turn, affect mid-latitude circulation. Over the Indian Ocean negative SLP anomalies prevail over most of the year, and only small (less 0.5 hPa) differences are found over the S. Atlantic Ocean. The Southern Ocean sector south of Australia experiences a small increase of SLP throughout the year at 6 kyr compared to PI.

As climate in the western coast of South America and Patagonia is strongly influenced by the South Pacific Anticyclone (SPAC), we calculated the annual evolution of the latitude of the maximum SLP in the South Pacific Ocean, as well as the value of this maximum for PI (black) and 6 kyr (pink), respectively, as a proxy for the SPAC evolution (Fig. 3e, f). These calculations indicate that the annual cycle of the intensity of the SPAC is amplified on the 6 kyr simulations and shifted one month ahead. In the PI simulation the minimum occurs between February and May, and the maxima in November, with an ~ 3 hPa amplitude, in contrast, the 6 kyr simulations show a minimum in April and a maximum in October with an amplitude of 4 hPa. The latitude at which the maximum SLP is centred, however, does not change; as with the intensity, this is shifted one month ahead in the 6 kyr simulations relative to PI.

3.3 Circulation

We examined the low (850 hPa) and upper (200 hPa) level winds to gain insights into the large-scale circulation changes in the SH (Figs. 4, 5). The largest changes are found over the Pacific Ocean during MAM and SON. During MAM strong positive and negative wind differences develop between 20–40°S and 40–60°S, respectively at 6 kyr compared to PI. The opposite condition is evident during SON. These changes are consistent with the differences in SLP described previously (Fig. 3). The annual mean shows a small but consistent equatorward shift (1–3°) of the latitude of maximum wind speed over the entire SH (simulated by 9 out of the 13 models, and statistically significant), which results in a small increase of wind speed over the South Pacific and Atlantic Oceans north of ~ 50°S and a widespread decline south of ~ 50°S.

The model mean seasonal and annual mean upper level winds (200 hPa) (Fig. 5) capture the main upper-level jets of the SH: the Subtropical Jet (STJ) during MAM and JJA, and the Sub Polar Jet (SPJ) during SON and DJF. As for the low-levels winds, the largest differences are seen in MAM and SON. In general for the four seasons, the pattern of changes are confined to each basin, including a decreased STJ over the Pacific Ocean in JJA and SON and an increase over South America in SON at 6 kyr compared to PI. The SPJ over the Pacific Ocean is increased both in DJF and SON, and decreased in DJF and MAM in the Australian sector. The changes in the SPJ are found through the troposphere, and manifest in the low-level circulation (Fig. 4). In the annual mean, in the 6 kyr simulations we observe a small decrease in the core region of the STJ and a small increase of the SPJ over the South Pacific and Atlantic Oceans compared to PI.

3.4 Precipitation

Figure 6 shows the ensemble model mean seasonal and annual precipitation difference (6 kyr-PI). The largest change is a decline of precipitation over the continents north of 40°S during summer (DJF) in the regions of the South African, Australian and South American Monsoon. In the 6 kyr simulations reduced precipitation during summer is also evident in relatively restricted areas of the Indian Ocean sector of the Southern Ocean, the SW Pacific, the southern tip of NZ (~ 47°S), and the Antarctic Peninsula; the remaining regions of the southern mid-latitudes exhibit increased precipitation over this season. During MAM we observe a broadly similar, but weaker pattern that in DJF, except south of 50°S, where precipitation anomalies are weakly negative, instead of positive. Drier conditions prevail during winter, except for low latitude (north of 20°S) Africa, Indonesia, NW South America; discontinuous zones in the Indian, Atlantic, and western Pacific Oceans between 30 and 45°S; and several parts of Antarctica. During spring precipitation increases over the Southern Africa, Australian and SA Monsoon regions; as well as in the southern parts of NZ and Patagonia. In the mid-latitudes the precipitation changes are consistent with the low-level wind changes discussed before, with more (less) precipitation north (south) of 45°S in MAM and the inverse in SON. In the annual mean, the subtropical to mid-latitudes continental regions are drier at 6 kyr compared with PI, and the ocean basins are wetter. Patagonia is slightly wetter whereas NZ is drier.

Figure 7 shows the difference (6 kyr-PI) in the amplitude of the annual cycle of precipitation (precipitation amounts differences in the months of maximum and minimum precipitation). It indicates very clearly the reduced amplitude of the annual cycle of precipitation of the monsoon regions (South Africa, Australia and South America), due to the reduction in summer precipitation (rainy season). This reduction is accompanied by an increase over the nearby oceans. South of about 40°S, there is a fairly homogeneous decrease in the amplitude of the annual cycle of precipitation. Except at the two "topographic barriers" south of 40°S: Patagonia and NZ, and some parts of Antarctica. However changes over Antarctica are not meaningful, due to low annual precipitation in the region.

3.5 Patagonia

Figure 8 shows the model mean seasonal mean 850 hPa winds (vectors), precipitation differences (colours) and SLP differences (contours), centred over the South American continent, from 40 to 100°W. These results show increased precipitation in South America during DJF and MAM in the region between 38 and 48°S, related to

Fig. 4 Model mean low level (850 hPa) zonal wind changes: 6 kyr-PI, **a** DJF, **b** MAM, **c** JJA, **d** SON, **e** Annual mean. In contours: 6, 8, 10 and 12 m/s zonal wind. In **e** *red* and *green line* latitude of maximum wind speed for PI and 6 kyr simulation respectively
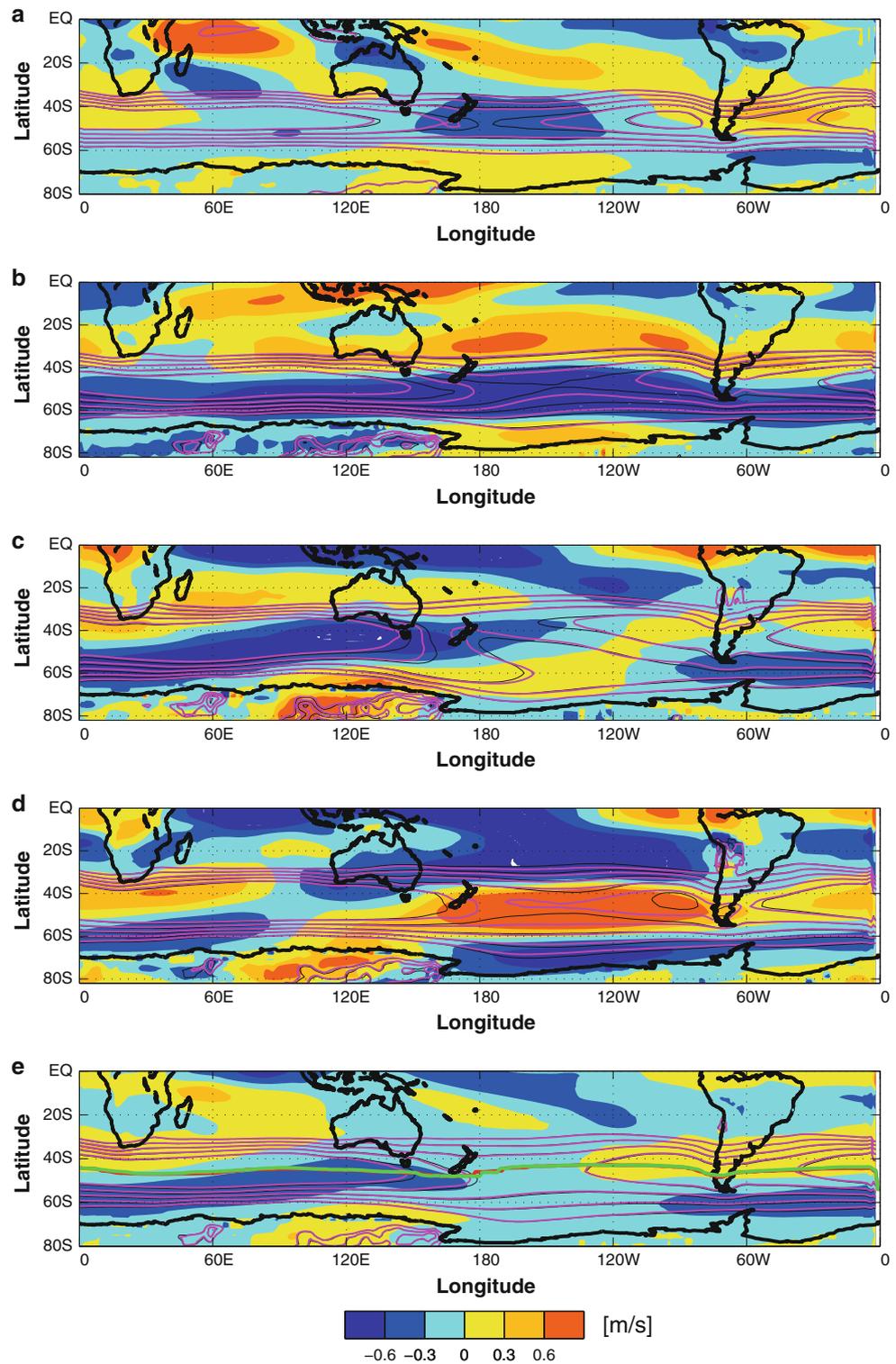
stronger northwesterly flow. This flow is part of an anti-cyclonic wind anomaly, around a negative SLP anomaly, that is centred at about 100°W. At the southern flank of this SLP anomaly, easterly wind anomalies are accompanied by less precipitation (south of 50°S). Conversely, less

precipitation during MAM and JJA between 48 and 60°S is coupled with easterly wind vector anomalies, i.e. weaker westerlies.

During SON, a dipole in precipitation change develops north and south of 45°S. North of 45°S, less precipitation is

Fig. 5 Same as Fig. 4, but for 200 hPa
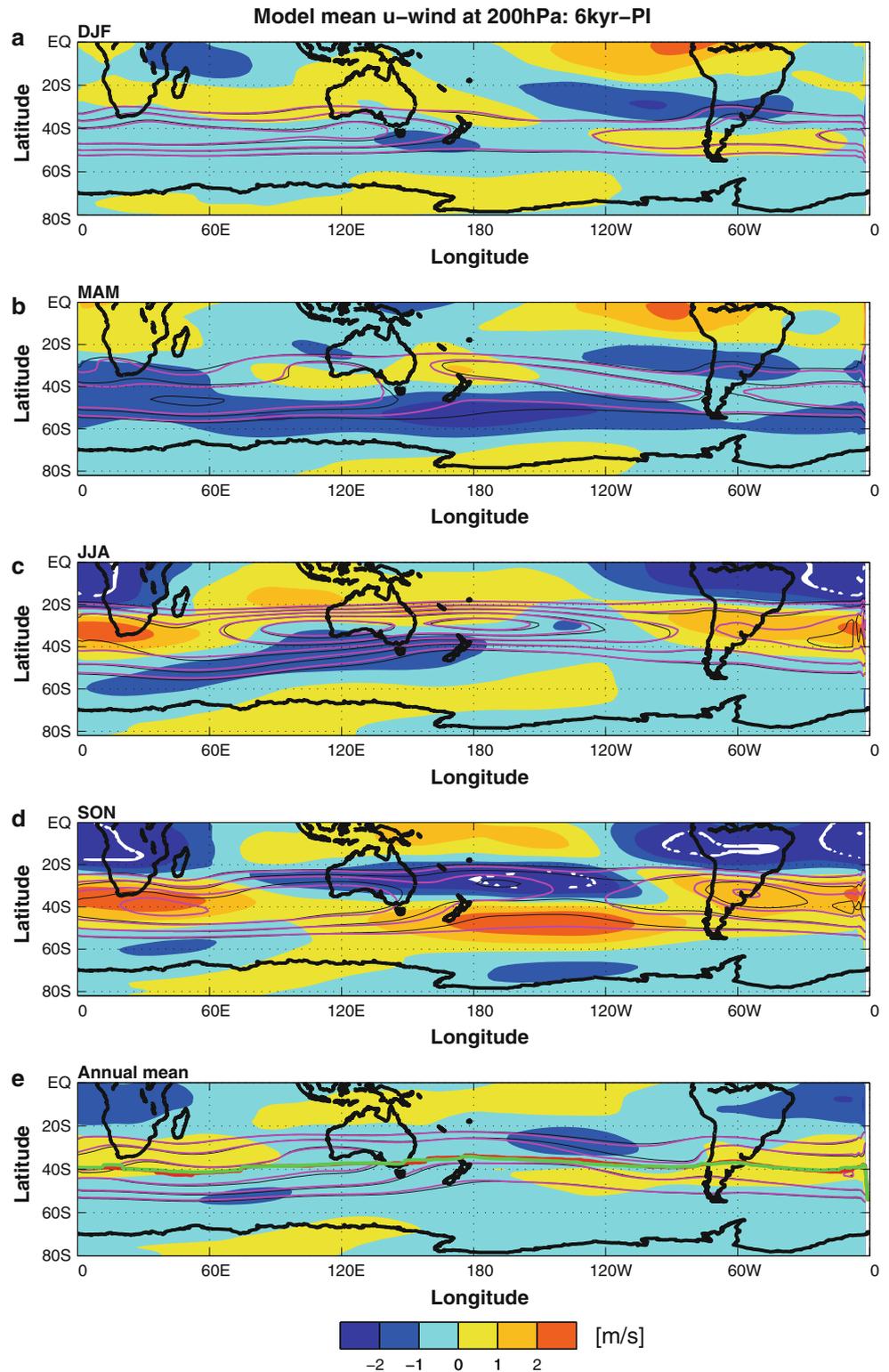
simulated at 6 kyr compared to PI, positive SLP are centred around 100°W and 35°S, that in turn produce anti-cyclonic circulation anomalies. South of 45°S, more precipitation is simulated, negative SLP anomalies are centred around 100°W and 60°S, which produce cyclonic circulation anomalies. These circulation anomalies manifest in an intensification of the surface westerly flow between 40 and 55°S. The annual mean (not shown) reveals enhanced westerly flow between 35 and 45°S, a weakening south of 45°S, and increased precipitation throughout Patagonia (38–50°S).

Fig. 6 Model mean precipitation differences, 6 kyr-PI: **a** DJF, **b** MAM, **c** JJA, **d** SON, **e** anual mean
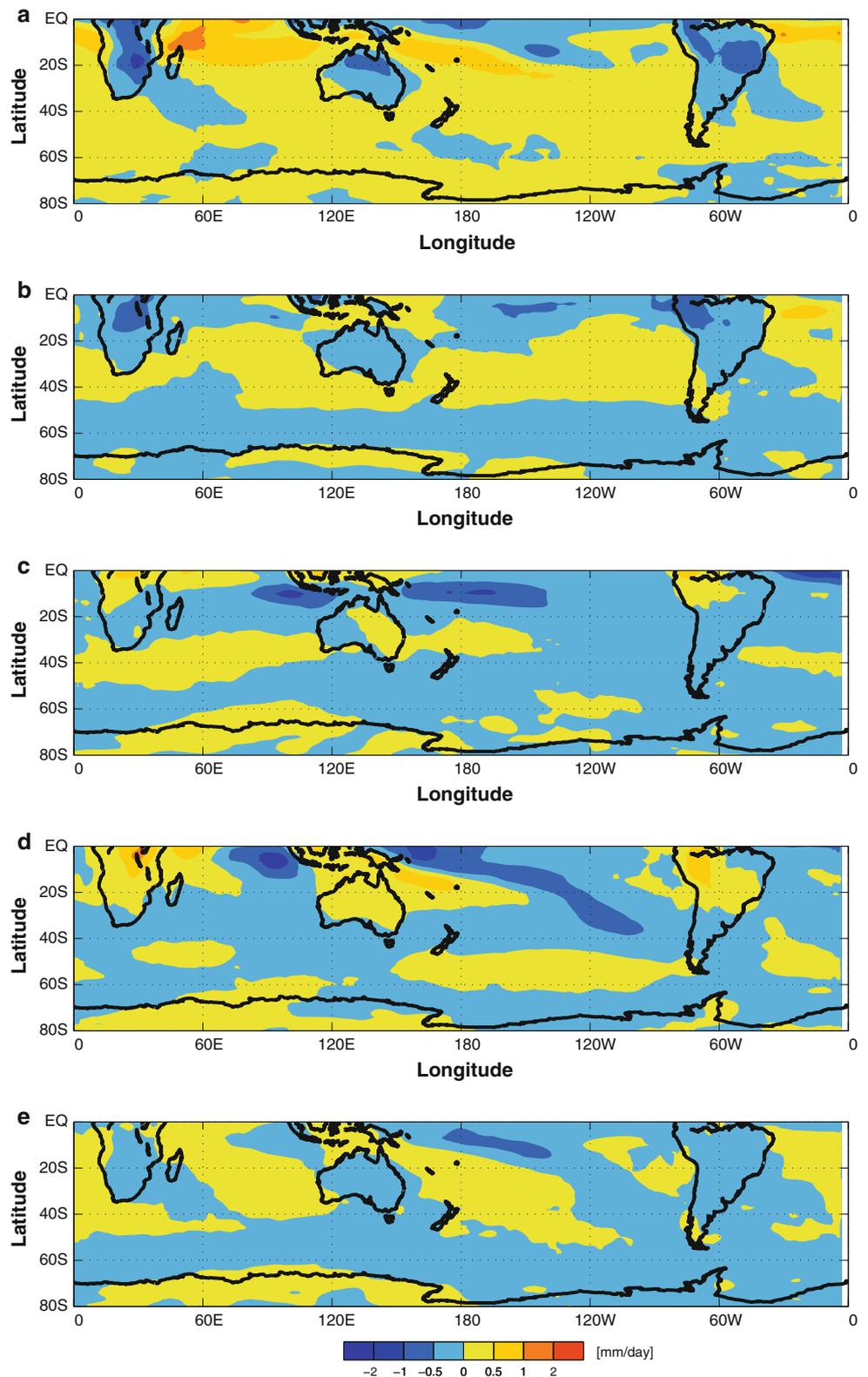
Figure 9 shows the monthly maximum wind speeds, the latitude of those maxima in the SE Pacific region (80°W). Their respective 6 kyr-PI differences are shown as boxplots. Maximum wind speeds decrease from January to July, and increase during August to December in the 6 kyr simulations. Furthermore, the latitude of maximum wind

Fig. 7 Model mean difference of the amplitude of annual precipitation cycle: 6 kyr-PI. Amplitude is defined as: precipitation amounts differences in the months of maximum and minimum precipitation
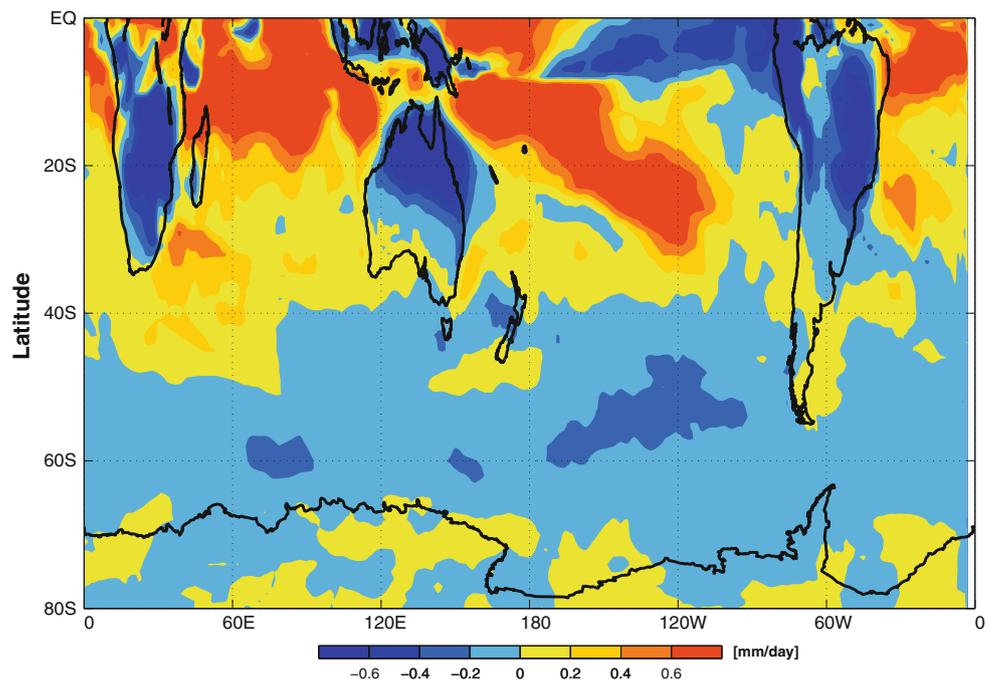
speeds shifts equatorward during March to May and moves slightly poleward during September to November. Figure 9c, d shows the inter-model spread of the differences, and indicate that maximum wind speeds differences are significant in all months, whereas the latitude differences are only appreciable during April and October. These changes are consistent with the changes in the annual cycle of SPAC shown in Fig. 3. In sum, the aforementioned precipitation anomalies over Patagonia imply a increased annual cycle in precipitation, i.e., less evenly distributed precipitation, that was slightly higher at 6 kyr than at present.

3.6 New Zealand

The New Zealand region, especially South Island, is also under the year-round influence of the southern westerlies in the modern climate. Figure 10 shows the model mean difference of 850 hPa wind vectors, SLP contours and precipitation in colours. More precipitation over NZ in DJF and MAM is associated in both seasons with negative SLP anomalies, cyclonic circulation anomalies and colder temperatures. We found positive SLP anomalies and anti-cyclonic circulation anomalies south of Australia during JJA and SON. This circulation anomaly is accompanied with negative SLP anomalies south of NZ during SON, leading to anomalous south-westerly flow and more precipitation in the southern part of South Island. This synoptic pattern resembles the anomalous conditions related to the twentieth century advance of Franz Joseph glacier, as shown in Figure 5 of Hooker and Fitzharris (1999). The

6 kyr simulations, however, indicate warmer than present conditions during JJA and SON in contrast to the colder condition described in Hooker and Fitzharris (1999).

Figure 11 shows the monthly maximum wind speeds, the latitude of those maxima, and their respective 6 kyr-PI differences in the Australia-NZ region (170°E). The low-level wind speed PI data shows maxima occurring in April and October (14 and 15 m/s, respectively) and minima during January and July (11 and 12 m/s, respectively). The annual PI cycle of the low-level winds features a south-ernmost position ($\sim 53°$S) between April and June, and a maximum equatorward position during August and September ($\sim 54°$S). The 6 kyr simulations show weaker low-level winds from January through July, and stronger from September until November, similar to the pattern observed at 80°W (Patagonia). We find no statistically significant change in the latitudinal position of the maximum wind speeds compared to the control simulations (Fig. 11c, d).

3.7 Estimation of snow

Although all models are capable of simulating surface snow thickness, below-freezing temperatures over the Southern Andes and Southern Alps are rarely reached and, consequently, the snow thickness values are zero in all models with the exception of HadCM3. This is partly due to the smoother and lower topography caused by the coarse spatial resolution of the models. Therefore, as a way to estimate snowfall we have corrected temperature by lapse rate and real altitude of the Andes and Alps at each grid-point, using the following relationship:
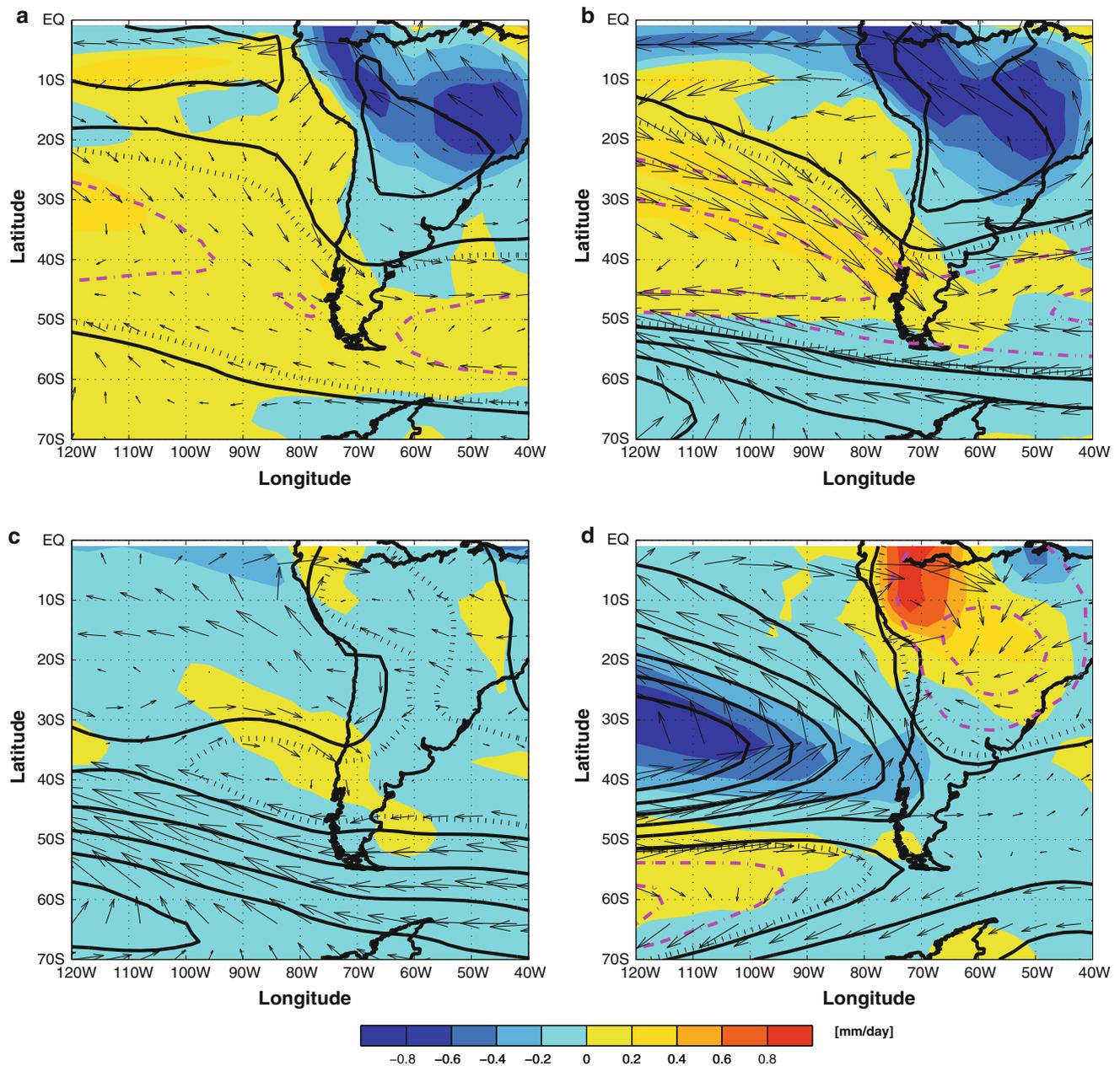
Fig. 8 Model mean wind vectors at 850 hPa, precipitation differences in colours, and SLP differences in contours (*black* positive, *magneta* negative, *dotted*: zero contour; other contours every 0.4 hPa). **a** DJF, **b** MAM, **c** JJA, **d** SON

$$T_{corr} = T_{model} + (H_{model} - H_{real}) \times 0.0065, \qquad (1)$$

where H_{model} is the mean elevation (m) of the model at each grid point, and H_{real} the mean elevation of the real topography, at 1 km resolution. T_{model} is the model temperature and T_{corr} the corrected temperature.

Figure 12 shows the annual cycle of the model mean T_{model} and T_{corr} averaged over Patagonia, as defined in Sect. 2. The lower panel shows the annual precipitation cycle for the same area. The vertical lines indicate the period where temperatures in Patagonia are below freezing

for the corrected temperatures, and therefore the time of year when precipitation can fall as snow. Note that the changes in the length of below freezing temperatures are of similar order of magnitude (days) than the error in the length of the season introduced by the model setup that was chosen for the 6 kyr simulations (Sect. 2.1).

Below-freezing T_{model} occur briefly during July in the PI simulation, and during June–July at 6 kyr. In contrast, T_{corr} shows freezing temperatures (hence snowfall) from mid May until the beginning of September in PI. Overall colder conditions are simulated at 6 kyr from December

Fig. 9 Model mean Annual cycle at 80°W of: **a** maximum wind speed, **b** latitude of maximum wind speed, for PI (*black*) and 6 kyr (*magneta*) simulation. **c** 6 kyr-PI difference of maximum winds speed, multi-model median (*red*), inter-quartile range (*blue*) and outlier (*red plus*) statistics shown as *boxplots*. **d** same as **c**, but for the difference in latitude of maximum wind speed
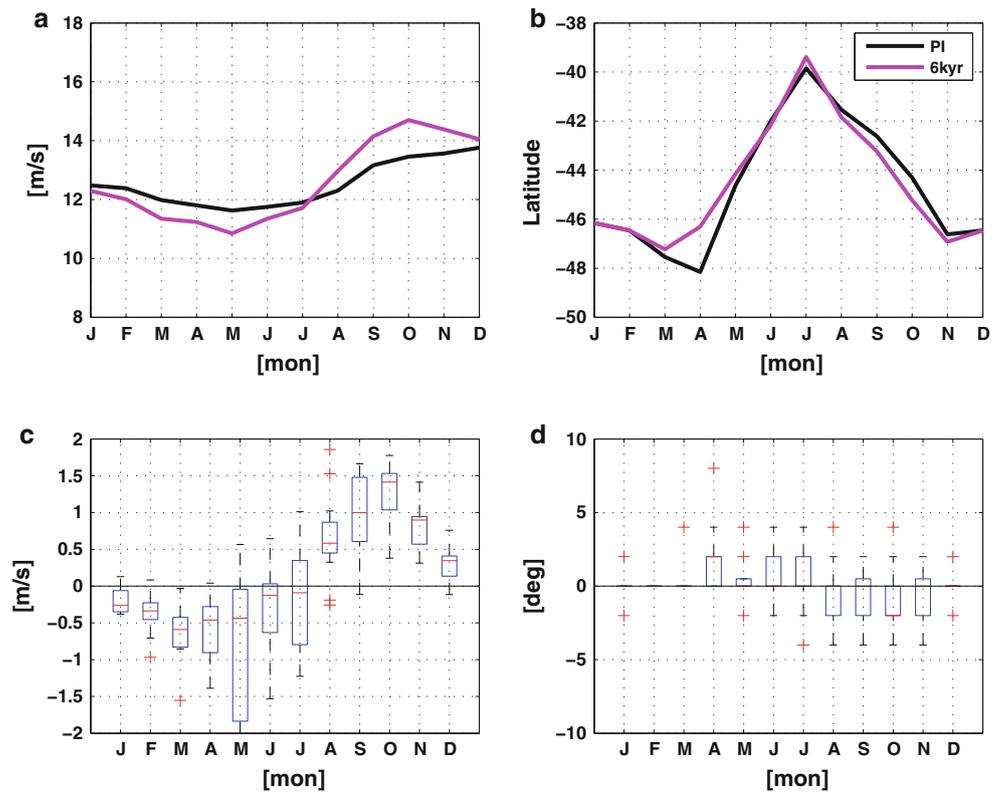
through August, and warmer conditions from September to November, the period with temperatures below zero is marginally longer at 6 kyr (starts two weeks earlier and ends one week earlier). In terms of precipitation, the 6 kyr simulations show more precipitation from September until May, and less between May and September, coinciding with the period of below-freezing temperatures. These results suggest that less precipitation felt during a colder accumulation season, and more precipitation felt during a warmer ablation season. A mass balance study of the Brewster Glacier, in South Island NZ (Anderson et al. 2010) indicates that a 50% increase in precipitation is required to offset a 1 degree warming. This is in agreement with a modelling study of the Franz Josef glacier which concluded that temperature is the dominant control on glacier length in this temperate mid-latitude setting (Anderson and Mackintosh 2006). In the context of these findings, the results of the 6 kyr simulations discussed above suggest on a qualitative basis that the temperature and precipitation anomalies could effectively lead to neoglacial advances in Patagonia and NZ, even if the annual precipitation was lower in NZ at 6 kyr, compared with PI. One should remember that analysis of temperature and precipitation anomalies at 6 kyr, compared to PI, was carried out with monthly mean data (as opposed to daily data), which could also result in

differences in the outcome of the annual cycle of snow accumulation/melt that we want to estimate. A quantitative approach using high-resolution climate and glaciological simulations should be conducted to assess this point in detail.

With respect to the annual corrected temperature cycle, the 6 kyr simulations show maximum temperatures shifted one month ahead relative to PI, but the timing of minimum temperatures remains invariant. We find no clear shift in the annual precipitation cycle, except that the 6 kyr simulations show minima in April and September. These changes lead to a slight increase in the annual temperature and precipitation cycles over Patagonia.

An equivalent correction of temperatures over NZ is shown in Fig. 13. Due to the lower elevation of the Southern Alps, compared to the Southern Andes, and the coarse resolution of the models, monthly mean temperatures in this region do not reach freezing levels, even with the altitude correction. Averaged over the NZ region, the 6 kyr temperatures where colder than PI from January through August, and warmer from September through December (same as for Patagonia). Precipitation is slightly lower over most of the year except in September and October (same as for Patagonia). These changes also lead to a slight increase in the annual temperature and precipitation cycles over NZ.
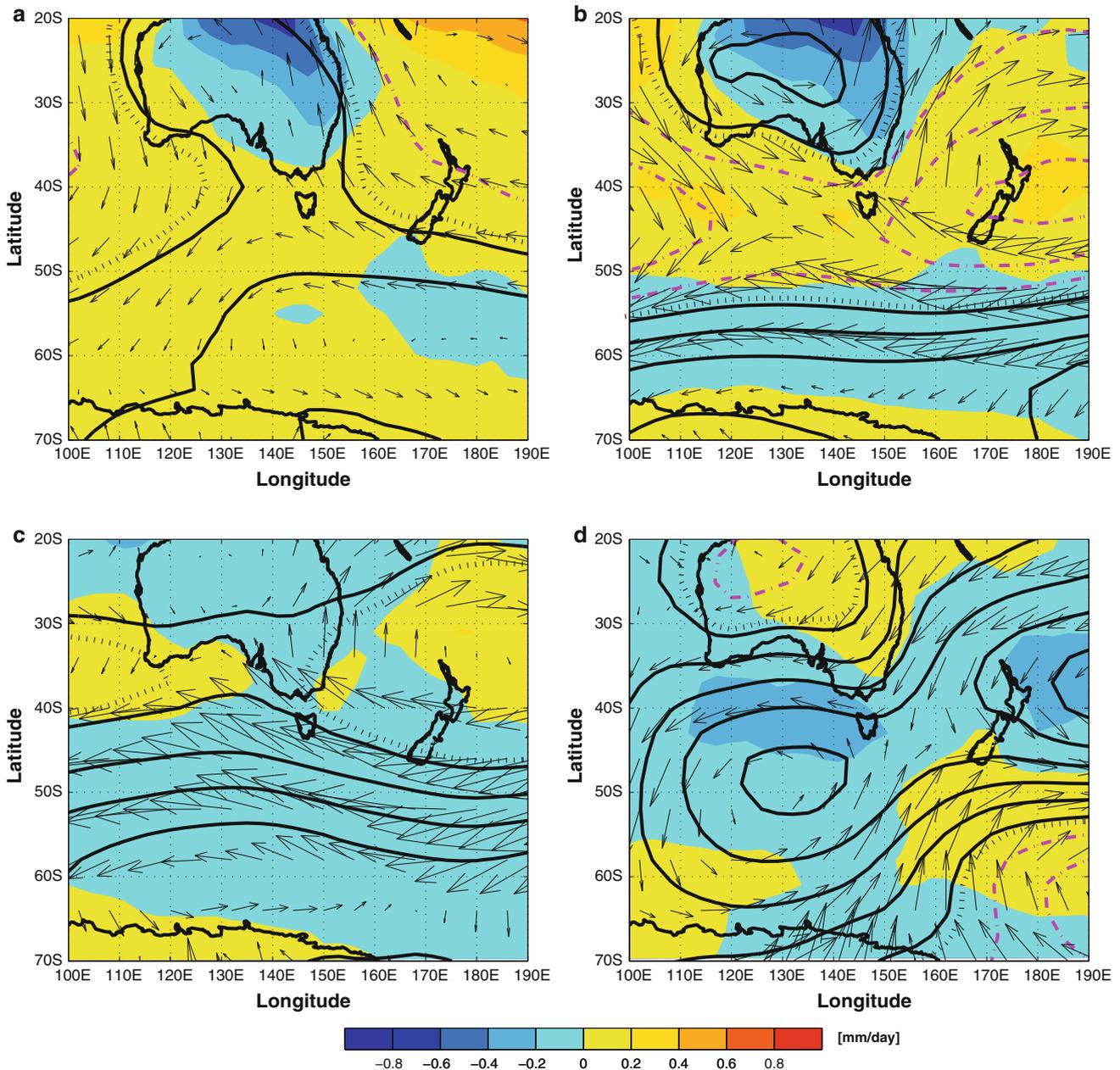
Fig. 10 Model mean wind vectors at 850 hPa, precipitation differences in *colours*, and SLP differences in contours (*black* positive, *magneta* negative, *dotted* zero contour; other contours every 0.4 hPa). **a** DJF, **b** MAM, **c** JJA, **d** SON

3.8 Radiation and cloud cover

Figure 14 shows the annual cycle of surface net incoming shortwave radiation and total cloud cover averaged over the Patagonia and New Zealand sectors, respectively. In both regions, the radiation curves mimic the insolation changes at these latitudes, with less insolation from January through June and more from July to November. There is no significant changes in total cloud cover. In Patagonia both the PI and 6 kyr simulations, the total cloud cover ranges around 68% in summer to 72% in winter. In New Zealand

the total cloud cover ranges between 56% in summer to 67% in winter. The radiative forcing at the surface is therefore similar to the insolation forcing at the top of the atmosphere.

4 Discussion

In this paper we analysed the complete PMIP2 simulations of the 6 kyr climate and focused our analysis on the Southern Hemisphere mid-latitudes, with emphasis on the

Fig. 11 Same as Fig. 9 but for model mean Annual cycle at 170°W
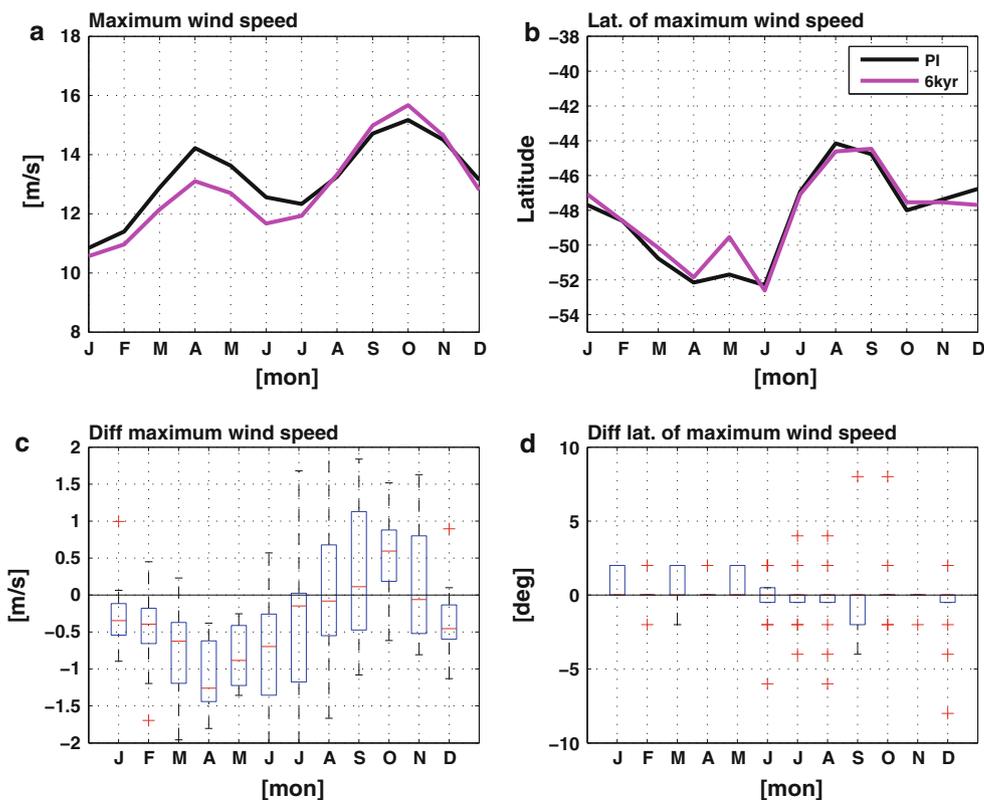
southern South American (Patagonia) and New Zealand regions (NZ), to gain insights into the observed neoglaciations in these regions. The major differences in SH climate at 6 kyr are found during spring (SON) and autumn (MAM), with relatively minor changes during the austral summer or winter. It is interesting to note that paleoclimate modelling studies have usually emphasised the diagnosis and analysis of past summer and winter conditions, approach that would have led us to overlook or miss key subtle changes in the PMIP2 simulations centred at 6 kyr.

Unlike the Northern Hemisphere, the annual insolation cycle in the SH did not experience significant changes in its amplitude; the largest insolation changes include negative anomalies during MAM and positive anomalies in SON. These changes led to reduced annual temperature and precipitation cycles over most continental areas, and slightly increased in Patagonia and NZ. The simulated changes in temperatures over the SH follow the insolation changes, with the expected 1–2 month delay over the oceans due to the thermal inertia of the later. Large-scale circulation features, such as the low and upper level winds and the subtropical anticyclones show an amplified annual cycle, as a direct response to the increased/decreased insolation during the transition seasons SON/MAM. We detect a small but consistent equatorward shift of the latitude of maximum wind speed of 1–3° over the entire SH in the annual mean (simulated by 9 out of the 13 models, and

statistically significant), which results in a small increase of low-level wind speed over the South Pacific and Atlantic Oceans north of ∼50°S, and a widespread decline south of ∼50°S.

The 6 kyr time-slice in the SH is immersed in a transitional phase from the multi-millennial peak warmth and precipitation minima of the early Holocene (10.5–7.8 kyr) to peak neoglacial (cool-temperate and wet) conditions in the late Holocene (5–2.7 kyr). Terrestrial paleoclimate studies from Patagonian regions sensitive to westerly wind variability indicate the onset of a trend toward increased precipitation, i.e., stronger wind speeds, and lower temperatures at ∼7.8 kyr. Millennial-scale changes in precipitation, including accentuations and reversals until ∼2.7 kyr, point to a highly dynamic ocean–atmosphere system throughout the Holocene. This variability was concurrent with advances of mountain and outlet glaciers from the Patagonian Ice-fields during neoglaciations. In NZ, glacier advances began ∼6300 years ago (Schaefer et al. 2009), but dates have important uncertainties associated (Porter 2000). PMIP2 simulations indicate that at 6 kyr NZ was colder and drier in the annual means, and exposed to weaker westerly winds. Patagonia was colder in the annual mean (between 38 and 50°S), there was more precipitation, together with stronger low-level winds. Approximately 1000 km north of NW Patagonia, in Central Chile (33°S), two lowland sites

Fig. 12 Model mean surface temperature (**a**) and mean precipitation (**b**) averaged over Patagonia
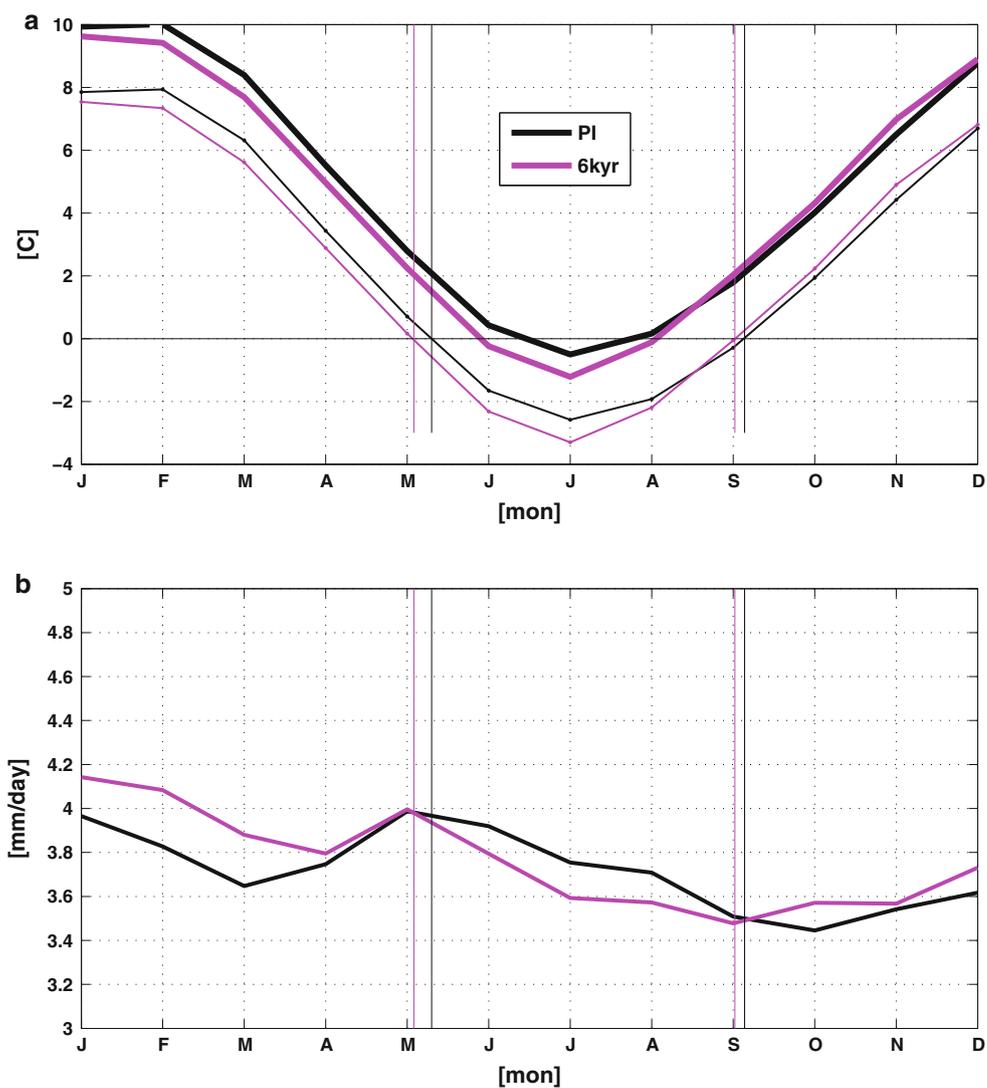
show a lake transgressive phase starting at 5.7 kyr indicative of an increase in precipitation of westerly origin. This ~2000 yr lag in precipitation rise recorded in the northern sites relative to the Patagonian records, might reflect the cumulative effect of a series of accentuations in westerly wind strength/latitudinal displacements (events dated at 7.8, 6.8, and 5.7 kyr). This delayed response might reflect that a critical climate boundary between these regions prevailed between 7.8 and 5.7 kyr, in fact, the 6 kyr simulations indicate that NW Patagonia and central Chile are in anti-phase with respect to temperature changes in the annual mean. Central Chile, was warmer and experienced less precipitation at 6 kyr compared to PI.

Palynological records from Tierra del Fuego indicate the expansion of Southern Beech (Nothofagus) forests, interpreted as the onset of a rising trend in precipitation at ~6.5 kyr (Heusser 1993; Markgraf 1993), following a

multi-millennial dry interval during the early Holocene. Subsequent studies (Gilli et al. 2005) proposed the onset of a dominant and permanent influence of the westerly winds in Lago Cardiel (49°S), located in the extra Andean region of central Argentinean Patagonian, at 6.8 kyr. More recently, Waldmann et al. (2009) reported geophysical data from sediment cores collected from Lago Fagnano (54°S, the largest lake in Tierra del Fuego), and interpreted the iron intensity data as evidence for a local increase in wind strength sometime after ~7.5 kyr. The fact that the negative anomaly in precipitation during the early Holocene and its subsequent change toward positive anomalies at ~7.8 kyr was symmetrical in areas north and south of the area of maximum westerly wind speeds and precipitation in Patagonia (45–53°S), led Moreno et al. (2010, in press) to propose that the strength of the southern westerlies, and not their latitudinal position, varied at multi-millennial timescales during the Holocene.

Fig. 13 Model mean surface temperature (**a**) and mean precipitation (**b**) averaged over New Zealand
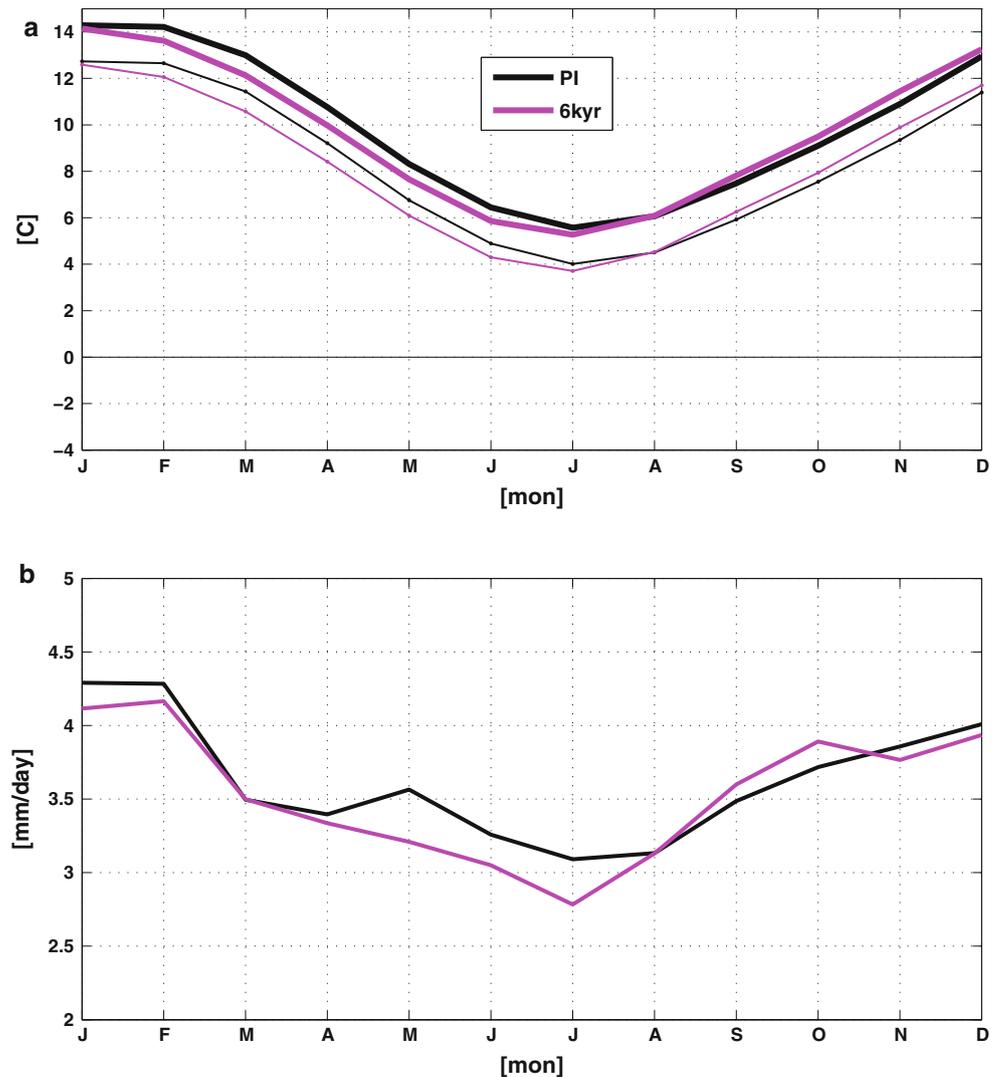
The PMIP2 results are consistent with the modelling results of Wagner et al. (2007). The aim of that analysis was to investigate the linkage between large-scale circulation and precipitation in the extra-Andean region of SE Patagonia (52°S, 70°W). Their transient simulation spanned the interval between 7 and 4.5 kyr and found that stronger SH westerly winds and lowered precipitation prevailed during the austral spring and summer, weaker winds and increased precipitation during the austral autumn and winter, and a moderate increase in annual precipitation. Their transient simulation also indicated a stronger seasonal variability of the SH westerlies compared to PI conditions.

In summary, both Patagonia and NZ received less precipitation during a colder accumulation season, and more precipitation during a warmer ablation season, leading to a slight increase in their precipitation seasonality (less evenly distributed precipitation) at 6 kyr, compared with PI. If temperature is the dominant control on glacier length in this temperate mid-latitude setting (Anderson et al, 2010), then the results of the 6 kyr simulations suggest, on a qualitative basis, that the temperature and precipitation anomalies could effectively lead to neoglacial advances in Patagonia and NZ. Moreover, there is an elevational control on the seasonality of glacier response—i.e., glaciers extending down to sea level might be sensitive to temperature changes throughout the year (even winter) whereas high mountain glaciers will mostly respond to changing summer temperatures (Oerlemans and Reichert 2000). A quantitative approach using high-resolution climate and glaciological simulations should be conducted to assess this point in detail.

The objective of this study was to gain insights into the observed neoglacial activity in the southern mid-latitudes. There are a number of "scale" issues (temporal and spatial) between the database analysed (AOGCM PMIP2 simulations) and the phenomenon intended to study (annual cycle of snow accumulation/melt) that should be highlighted.
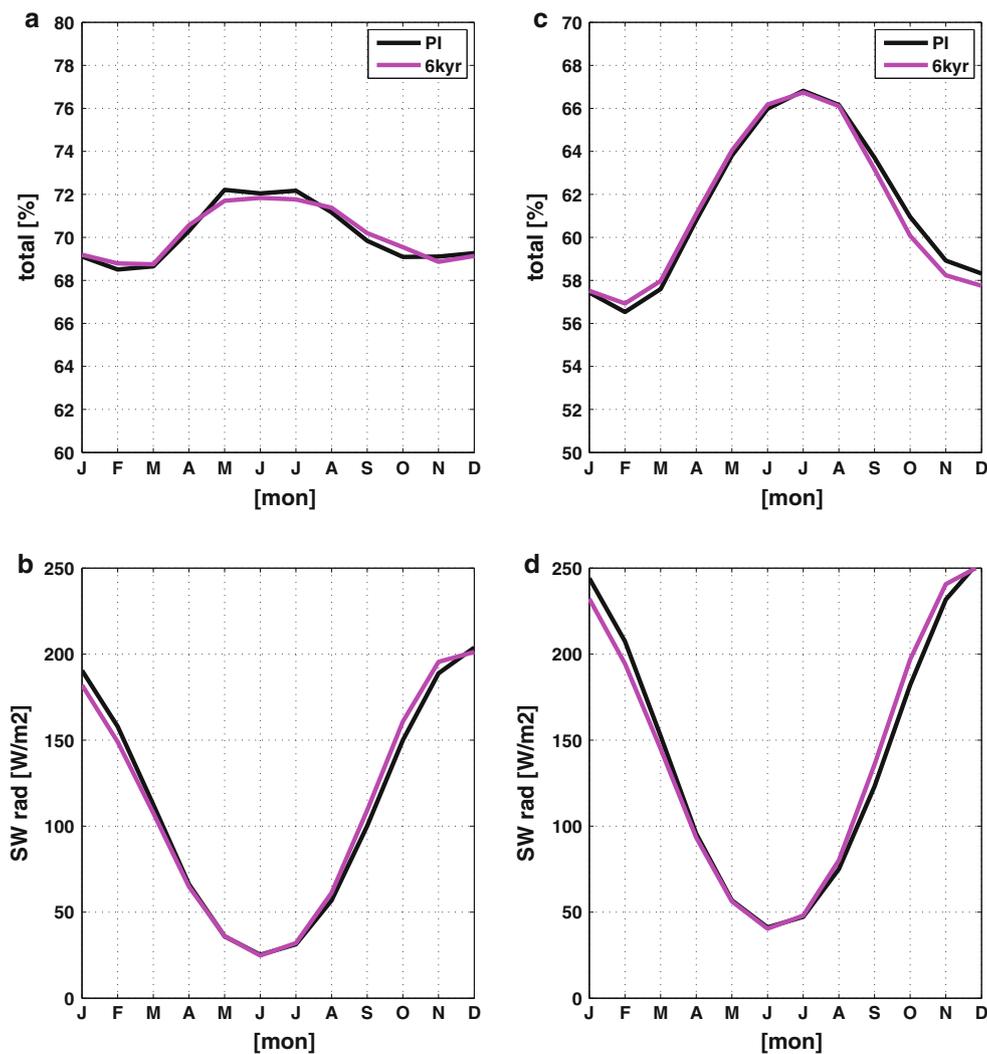
Fig. 14 Model mean annual cycle of total cloud cover and of shortwave radiation averaged over Patagonia and New Zealand. **a** Total cloud area fraction (73–69 W, 46–53 S). **b** Surf downwelling SW radiation (73–69 W, 46–53 S). **c** Total cloud area fraction (170–180 E, 43–48 S). **d** Surf downwelling SW radiation (170–180 E, 48–43 S)

(1) Given the spatial coarseness in most of the models analysed, the topographic effect on precipitation is not well captured and, therefore, the real precipitation response to the 6 kyr forcing could possibly be missed in the particularly narrow mountainous regions of NZ and Patagonia, leading to a weaker response. (2) The atmospheric response of the southern mid-latitudes to SON forcing is probably overestimated, considering that the paleoseasons were defined using the same calendar duration as the control simulation in the PMIP2 setup protocol (Braconnot et al. 2007a). Hence the simulated warming in the accumulation season would be overestimated, which would also disfavour snow accumulation. (3) Analysing monthly mean data (as opposed to daily data) could also potentially alter the results of the annual cycle of snow accumulation/melt that we want to estimate.

5 Conclusions

Our analysis of the ensemble mean of 13 coupled ocean–atmosphere simulations carried out in the context of the PMIP2 initiative suggests that cooling and increased precipitation during the ablation (DJF) season, along with slightly higher precipitation and temperature seasonality, could account for the well-documented neoglacial activity and climate changes in the southern mid-latitudes at 6 kyr.

A better understanding of neoglaciations in the SH at multi-millennial timescales will emerge from additional time-slices, such as the 9 and 3 kyr boundary conditions. These highly relevant time-slices should capture the full range of climatic variability associated with neoglaciations in the southern mid-latitudes, and could provide the basis for modelling biological, geochemical, and glaciological

processes during the present interglacial. Transient AOGCM simulations spanning the entire Holocene, as shown by Liu et al. (2009), would allow testing the time-dependency of neoglaciations and changes in the southern westerly winds to the rising trend in summer insolation and atmospheric CO_2 during this time interval.

References

Abarzua AM, Villagran C, Moreno PI (2004) Deglacial and postglacial climate history in east-central Isla Grande de Chiloe, southern Chile (43 degrees S). Quat Res 62:49–59

Anderson B, Mackintosh A (2006) Temperature change is the major driver of late-glacial and Holocene glacier fluctuations in New Zealand. Geology 34(2):121–124. doi:10.1130/G22151.1

Anderson B, Mackintosh A, Stumm D, George L, Kerr T, Winter-Billington A, Fitzsimons S (2010) Climate sensitivity of a high-precipitation glacier in New Zealand. J Glaciol 56(195):114–128

Braconnot P, Otto-Bliesner B, Harrison S, Joussaume S, Peterschmitt JY, Abe-Ouchi A, Crucifix M, Driesschaert E, Fichefet Th, Hewitt CD, Kageyama M, Kitoh A, Laine A, Loutre M-F, Marti O, Merkel U, Ramstein G, Valdes P, Weber SL, Yu Y, Zhao Y (2007) Results of PMIP2 coupled simulations of the mid-Holocene and Last Glacial Maximum. Part 1: experiments and large-scale features. Clim Past 3:261–277

Fitzharris BB, Clare GR, Renwick J (2007) Teleconnections between Andean and New Zealand glaciers. Glob Planet Change 59:159–174

Gilli A, Ariztegui D, Anselmetti FS, McKenzie JA, Markgraf V, Hajdas I, McCulloch RD (2005) Mid-Holocene strengthening of the Southern westerlies in South America: sedimentological evidences from Lago Cardiel, Argentina (49°S). Glob Planet Change 49:75–93

Heusser CJ (1993) Late Quaternary forest-steppe contact zone, Isla Grande de Tierra del Fuego, subantarctic South America. Quat Sci Rev 12:169–177

Hooker BL, Fitzharris BB (1999) The correlation between climatic parameters and the retreat and advance of Franz Josef Glacier, New Zealand. Glob Planet Change 22:39–48

Joussaume S, Braconnot P (1997) Sensitivity of Paleoclimate simulation results to season definitions. J Geophys Res 102:1943–1956

Kutzbach JE, Liu Z (1997) Response of the African monsoon to orbital and ocean feedbacks in the Middle Holocene. Science 278:440. doi:10.1126/science.278.5337.440

Lamy F, Hebbelm D, Rohl U, Wefer G (2001) Holocene rainfall variability in southern Chile: a marine record of latitudinal shifts of the southern westerlies. Earth Planet Sci Lett 185:369–382

Liu Z, Harrison SP, Kutzbach J, Otto-Bliesner B (2004) Global monsoons in the mid-Holocene and oceanic feedback. Clim Dyn 22:157–182. doi:10.1007/s00382-003-0372-y

Liu Z, Otto-Bliesner BL, He F, Brady EC, Tomas R, Clark PU, Carlson AE, Lynch-Stieglitz J, Curry W, Brook E, Erickson D, Jacob R, Kutzbach J, Cheng J (2009) Transient simulation of last deglaciation with a new mechanism for Bolling-Allerod warming. Science 325. doi:10.1126/science.1171041

Markgraf V (1993) Paleoenvironments and Paleoclimates in Tierra-Del-Fuego and Southernmost Patagonia, South-America. Palaeogeogr Palaeoclimatol Palaeoecol 102:53–68

Massaferro J, Brooks SJ (2002) Response of chironomids to late quaternary environmental change in the Taitao Peninsula, southern Chile. J Quat Sci 17:101–111

Monnin E, Steig EJ, Siegenthaler U, Kawamura K, Schwander J, Stauffer B, Stocker TF, Morse DL, Barnola JM, Bellier B, Raynaud D, Fischer H (2004) Evidence for substantial accumulation rate variability in Antarctica during the Holocene, through synchronization of CO_2 in the Taylor Dome, Dome C and DML ice cores. Earth Planet Sci Lett 224:45–54. doi:10.1016/j.epsl.2004.05.007.228

Moreno PI (2004) Millennial-scale climate variability in northwest Patagonia over the last 15000 yr. J Quat Sci 19:35–47

Moreno PI, Francois JP, Villa-Martinez R, Moy CM (2010) Covariability of the Southern Westerlies and atmospheric CO_2 during the Holocene. Geology (in press). doi:10.1130/G30962.1

Oerlemans J, Reichert BK (2000) Relating glacier mass balance to meteorological data by using a seasonal sensitivity characteristic. J Glaciol 46:1–6

Porter SC (2000) Onset of neoglaciation in the Southern Hemisphere. J Quat Sci 15(4):395–408

Rojas M, Moreno P, Kageyama M, Crucifix M, Hewitt C, Abe A, Ohgaito R, Brady E, Hope P (2009) The last glacial maximum in the Southern Hemisphere in PMIP2 simulations. Clim Dyn 32:525–547. doi:10.1007/s00382-008-0421-7

Schaefer JM, Denton GH, Kaplan M, Putnam A, Finkel RC, Barrell DJA, Andersen BG, Schwartz R, Mackintosh A, Chinn T, Schluchter C (2009) High-frequency Holocene glacier fluctuations in New Zealand differ from the Northern Signature. Science:324:622–625

Shulmeister J, Goodwin I, Renwick J, Harle K, Armand L, McGlone MS, Cook E, Dodson J, Hesse PP, Mayewski P, Curran M (2004) The Southern Hemisphere Westerlies in the Australasian sector over the last glacial cycle: a synthesis. Quat Int 118–119:23–53

Wagner S, Widmann M, Jones J, Haberzettl T, Lücke A, Mayr C, Ohlendorf C, Schäbitz F, Zolitschka B (2007) Transient simulations, empirical reconstructions and forcing mechanisms for the mid-Holocene hydrological climate in southern Patagonia. Clim Dyn 29:333–355. doi:10.1007/s00382-007-0229-x

Waldmann N, Ariztegui D, Anselmetti FS, Austin JAJ, Moy CM, Stern C, Recasens C, Dunbar RB (2009) Holocene climatic fluctuations and positioning of the Southern Hemisphere Westerlies in Tierra del Fuego (54°S), Patagonia. J Quat Sci. doi:10.1002/jqs.1263

Whitlock C, Moreno PI, Bartlein PJ (2007) Holocene fire patterns in southern South America: present-day analogues for past periods of high fire activity. Quat Res 68:28–36

Wohlfahrt J, Harrison SP, Braconnot P (2004) Synergistic feedbacks between ocean and vegetation on mid- and high-latitude climates during the mid-Holocene. Clim Dyn 22:223–238. doi:10.1007/s00382-003-0379-4